FRACTURE PROCESS ZONE ANALYSIS OF CEMENTITIOUS MORTARS SUBJECTED TO CYCLIC LOADING

NUHAMIN E. DERESSE[*], MINA SAREM[*], STIJN FRANCOIS[*] AND ELS VERSTRYNGE[*]

[*] KU Leuven; Civil Engineering Department
Kasteelpark Arenberg 40 box 2448, 3000 Leuven, Belgium
e-mail: nuhamineshetu.deresse@kuleuven.be

Key words: fracture process zone; acoustic emission; digital image correlation; fatigue; Brazilian splitting test; cementitious mortar

Abstract: Fatigue is the progressive and irreversible change of the internal material structure due to repeated cyclic loading. These cyclic loads can result from wind, waves, temperature fluctuations, and traffic loads. Each load cycle introduces micro-damages that accumulate and eventually lead to failure. Detecting these micro-damages requires the use of sensitive measurement techniques. This is where advanced non-destructive testing (NDT) methods, such as acoustic emission (AE) and digital image correlation (DIC), play a vital role. Cylindrical mortar samples are subjected to a cyclic Brazilian splitting test. During the cyclic load, the damage evolution is monitored with AET and DIC. The progression of damage, measured through the cumulative count of acoustic emission events exhibited a strong correlation with the tensile deformation measurement obtained from Digital Image Correlation (DIC). The damaged region visualized with both techniques corresponds well. Subsequently, the size of the FPZ is measured using several AE-based and DIC-based methods. A comparison of the approaches indicated that the AE energy-based method is the most suitable to quantify the FPZ size during fatigue damage progress.

1 INTRODUCTION

Fatigue is the gradual increment of damage due to the application of repeated loadings. This damage is a result of progressive microcracking. In concrete, these micro-cracks are often detected using pulse velocity (ultrasonics), strain, and acoustic emission measurements [1].

When a material is going through an irreversible change such as micro-cracking, energy is released and part of this energy will generate transient elastic waves. These waves are called acoustic emissions (AE) and the technique of detecting and analyzing the source of AE is known as the acoustic emission technique (AET). AET is a highly sensitive technique used to detect microscopic changes in a material [2, 3]. Hence, AET can aid in early damage detection, which can ultimately help predict the material's fatigue life.

The challenges regarding the reproducibility of Acoustic Emission Testing (AET) results and the subjective nature of AET trend interpretation highlight the importance of comparing AET outcomes with other Non-Destructive Testing (NDT) techniques [4-6]. In this study, Digital Image Correlation (DIC) will be employed as a reference method for damage measurements. DIC is a non-contact and non-intrusive measurement technique used to obtain high-resolution full-field displacement and strain measurements [7]. While DIC analyzes material evolution through surface

deformation measurements, AET, on the other hand, is capable of monitoring damage within the volume of the material [8].

Fatigue fracture is governed by the formation of micro-cracks in the fracture process zone (FPZ). The FPZ is found near areas of stress concentration, where the material shows nonlinear behavior such as micro-cracking. Identifying this zone is useful in quantifying the material's fracture properties and understanding its behavior [1]. Researchers have used DIC [9-12] and AET [3, 13-16] to investigate the size of FPZ. Despite these applications of DIC, the effects of the user-defined variables such as subset size, step size, strain window, and strain limits on the DIC results introduce uncertainty and errors. There is also a lack of research work that compares the performance of the different approaches of AET in FPZ analysis. Therefore, in this paper both AE event count and AE energy approaches are applied and compared with DIC-based results.

2 EXPERIMENTAL PROCEDURES

2.1 Materials and specimen preparation

The cement mortars were made with a composition of 533 kg/m³ cement CEMII/B 26 (S-L) 32.5 N, 1600 kg/m³ river sand with a maximum aggregate size of 4 mm and 0/2 grain size curve distribution, and 266.5 l/m³ water. Tested according to NBN EN 196-1 [17], the mean and standard compressive strength is 20.65 MPa and 0.71 MPa respectively and the mean and standard flexural strength is 3.56 MPa and 0.33 MPa.

For the Brazilian splitting test, cylindrical mortar simple with a 27 mm diameter and a 27 mm length is prepared according to EN 12390-6 [18]. The load is distributed over load-bearing strips made from hardboard wood with a 3 mm thickness and 4 mm width.

2.2 Test setup and loading patterns

Brazilian splitting tests with step-wise fatigue loading were carried out on a universal testing machine (Shimadzu AG-X) with a maximum capacity of 100 kN. The test was a displacement-controlled test with a frequency ranging between 0.022 to 0.067 Hz and with a fixed upper and lower load limit. This load limit was defined as a percentage of the mean ultimate load obtained during monotonic tests on similar samples. After passing 50 cycles, the initial upper load limit was raised to a higher level and this process was repeated until failure was obtained. Because the number of load cycles are below 10^3 to 10^4 cycles, the fatigue loading is termed as low cycle loading [19]. The lower load limit remained fixed at 40 %. Because of the increasing load amplitude, the test is referred to as a step-wise fatigue Brazilian splitting test.

2.3 Acoustic emission (AE) monitoring

AE monitoring during the tests was carried out using six piezoelectric broadband AE sensors (Digital Wave B1025) with a 50 to 2000 kHz frequency range, see Figure 1 a). The sensors were chosen mainly due to their miniature size (9.3 mm diameter, 12.7 mm height), broadband response and adequate frequency range for the small samples. The AE sensors were mounted on the sample surface with a thin layer of hot-melt glue. The sensor layout is shown in Figure 1 b). The sensor layout is designed in such a way that the entire sample can be monitored while leaving the front surface available for the DIC monitoring. The AE sensors were connected to preamplifiers with 34 dB gain (AEP5, Vallen) and subsequently to a Vallen AMSY-6 acquisition system with six AE channels. The acquisition system digital frequency filter was set between 25 kHz to 850 kHz. An amplitude threshold of 40 dB is set to avoid capturing the background noises. This value is determined by monitoring the noises in the laboratory. The average wave velocity determined from UPV tests was 3650 m/s.
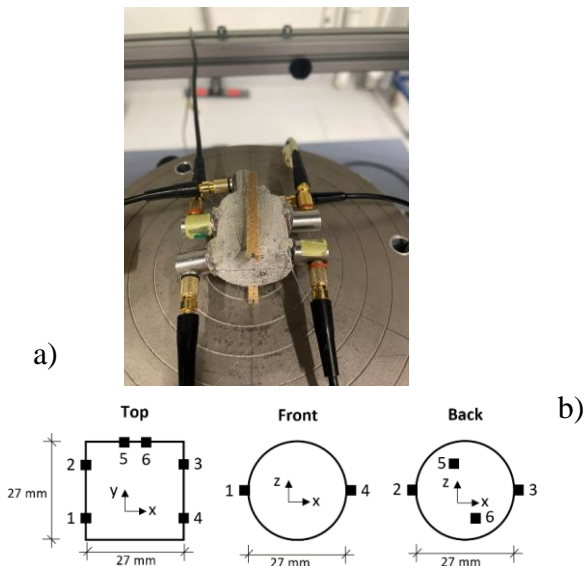
Figure 1 a) Test setup of the Brazilian splitting tests with AE monitoring technique b) AE sensor layout.

2.4 Digital image correlation (DIC) testing and analysis

Stereo-DIC was used to obtain a full-field displacement measurement of the region of interest (ROI), see Figure 2 a). The digital images were captured with two CCD Allied vision stingray cameras (F-504B/C firewire) equipped with 12 mm lenses. The cameras had a resolution of 2452 x 2056 pixels and 8-14 bit depth. For the stepwise fatigue tests, images were set to capture the circular surface of the cylindrical sample at 5-second intervals. The value of the interval was defined so that 3 to 5 images were taken per cycle. The cameras were mounted at a location where most of the field of view (FOV) was occupied by the sample and the resulting resolution was 40 µm/pixel. To increase the contrast and accuracy of tracing patterns between the reference and the deformed images, random speckle patterns were manually created by using 0.05 mm and 0.1 mm thick black pen, as done [20], see Figure 2 a). A commercial software called MatchID was used to capture, calibrate and perform the stereo-DIC analysis.
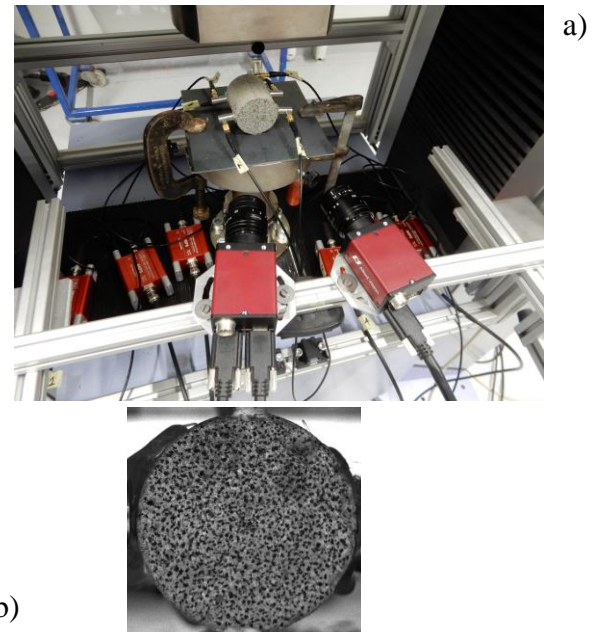

Figure 2 a) Test setup of the Brazilian splitting tests with AE and DIC monitoring techniques b) Speckle pattern for the DIC.

3   RESULTS

3.1 Cumulative fatigue damage analysis

The fatigue load cycle along with the cumulative acoustic emission event count and the vertical and horizontal deformations of the stepwise fatigue Brazilian splitting test is shown in Figure 3.

The initial elastic deformation of the sample (0 to 65%) is captured by the DIC vertical defamations measurement, see Figure 3. During this phase there are little to no AE activity and horizontal (tensile) deformation measured by DIC. This continues throughout the subsequent loading stages (40 – 65 %, 40 – 75 %, 40 – 80 %). Indicating that the sample did not experience much permanent deformation in these loading stages [21].

In the last loading stage (40 – 90%) the initiation of the progressive damages was captured after passing the 8th cycle. These damages were captured by the growth of the AE event count and the horizontal (tensile) deformation of the DIC measurements. After passing the 23rd cycle the sample failed by cracking vertically along the loading direction, see Figure 3.
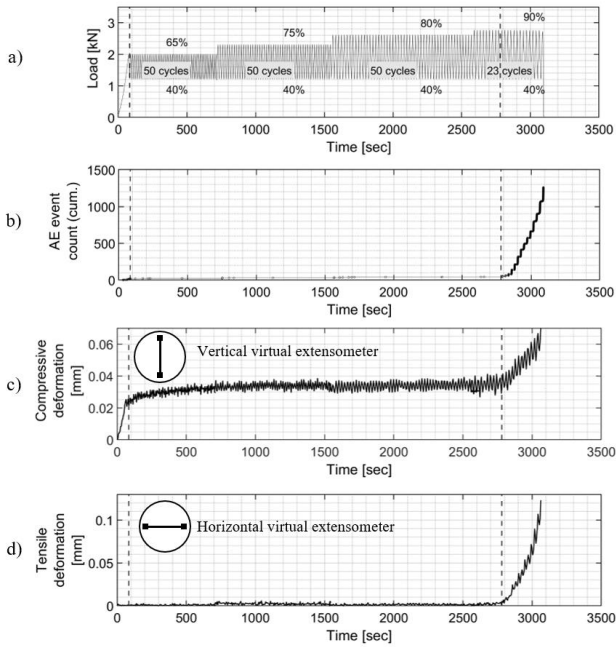
Figure 3 load-time curve a), cumulative AE event count b), compressive deformation c), and tensile deformation d) of a stepwise fatigue Brazilian splitting test of the small sample [21].

When comparing the normalized AE event evolution with time and the DIC-tensile deformation evolution with time a nearly identical damage growth pattern was captured by the two techniques, see Figure 4. Overall, when comparing the two techniques it was observed that, as a full field displacement measurement technique DIC is cable of detecting both elastic and inelastic changes. Meanwhile AE technique can detect irreversible or inelastic changes. Accordingly, the similarity in damage measurements seen in Figure 4 are the inelastic deformations measured by the two techniques. Evolution of fatigue and monotonic damage were performed using AE and DIC for samples with different sizes and is further discussed in [21].
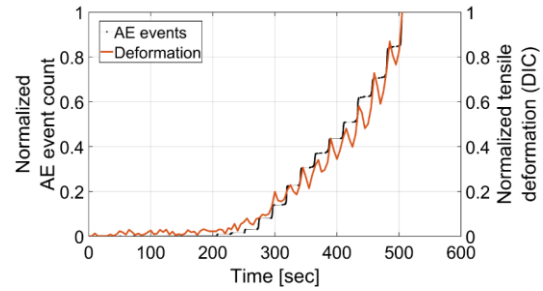

Figure 4 Relation between normalized DIC-based tensile deformation versus the normalized AE event count for the small sample [21].

3.2 Fracture process zone analysis

Figure 5 shows the localization plots of the AE event sources (red dots) overlaying on the horizontal displacement (u) field plot. The overall damaged region shown in Figure 5 is represented by the area with the high density of located AE events and the region with opposite signs of horizontal displacement. The horizontal displacement and the number of located AE events increases with each load cycle and a good agreement is found between located AE event sources and DIC results [21].
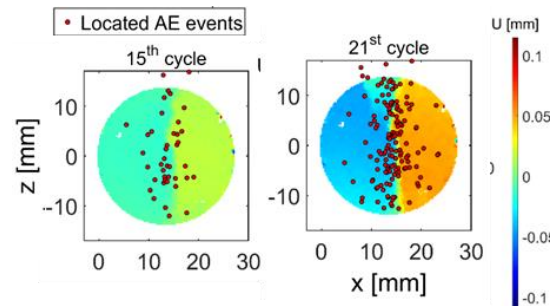

Figure 5 AE localization plot overlaying on the horizontal displacement (u) field plot obtained from DIC results at selected cycles in the final loading phase (the red dots represent the located AE events) [21].

4

The size of the fracture process zone (FPZ) is quantified using both DIC and AE techniques. The DIC results such as displacement field and strain fields are dependent on the user inputs, such as subset size(SS), step size(ST), strain smoothing window (SW) (i.e., number of virtual strain gauges (VSG) and spatial resulution (SR). Hence a study is conducted to investigate the effect of these parameters. Figure 6 shows the strain filed plot for a varying combination of SS, ST and SW. It can be seen for the cases with lower VSG (below 100) the width at certain strain level (shown in broken lines) converges to similar values as seen by the yellow, light-blue, orange, blue and purple colored lines. However for those with higher VSG (above 100) the value of the width at this strain level is higer, see the burgendy and the green colored lines. This is because for both of this cases due to a higher strain window (SW) (the burgendy) or higher step size (ST) (the green) there is higher smoothening of the spatial resulution which results in a wider strain distribution and lower maximum strain.

According here, the material strength, material heterogeneity, image resolution and speckle pattern characteristics were used to determine suitable parameters . Hence, the DIC analysis is performed using a subset size of 31x31 pixels (1.24 mm), and a step size of 7 pixels (0.28 mm). For image resolution of 40 μm/pixel and an average speckle size of 9 pixels, these values are chosen so that each subset has an average of three speckles, and one-fourth of the subset size is used to define the step size, this is according to recommendations by Jones and Ladicola [22].

The strain gauge size is set to be larger than the material heterogeneity. Accordingly, the size of the virtual strain gauge (VSG) was set to 100 pixels (4mm), or a strain window (SW) of 11 pixels, which is equivalent to the maximum size of heterogeneities in the samples, e.g., large pore or sand particle (max. 4 mm), this further elaborated in [21].
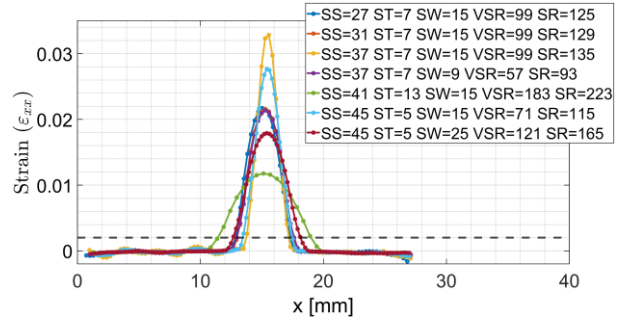

Figure 6 The effect of DIC parameters on strain field.

For AET the most common method of measuring the size of FPZ is using the histogram of the located AE events along the direction of interest see Figure 7. The histograms are built with a 2 mm interval along the x-axis.
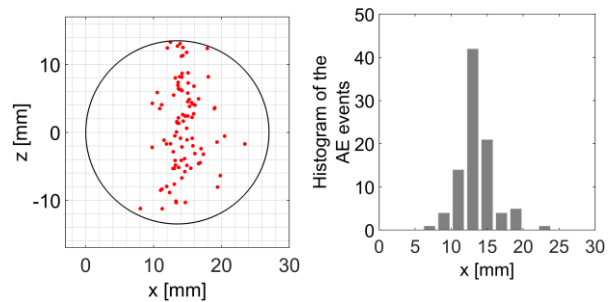

Figure 7 AE event localization plot and the histogram of the located AE events. (the located AE events are for a single loading cycle)

The localization plots of AE events and the strain field plots of DIC analysis are used to quantify the width of the fracture process zone. The strain field plots are used to analyze the FPZ. Figure 8 shows the strain field ε_{xx} plot at different cycles with a contour line showing the strain limit ($\varepsilon_{xx} = 0.77$ E-3). This strain limit is the sum of the limit tensile strain (0.22E-3) and the noise floor of the DIC analysis (0.55E-3). The estimation of the tensile strain limit values is discussed in detail in [21].
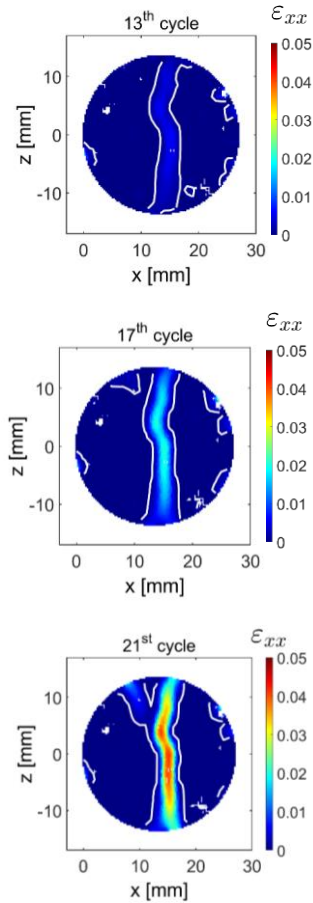
Figure 8 Strain field εxx plot at three peak loads of selected load cycles for the stepwise fatigue test with a contour line at εxx = 0.77 E-3 [21].

Figure 9 a) shows the εxx strain distribution at different cycles in the last stage of the stepwise fatigue test. The values of εxx on the x-z surface are averaged to give a single value at every 2 mm interval (along the x-direction). The fracture process zone (FPZ) is defined as the zone where the strain εxx is above 0.77E-3. This limit is shown as a dotted line in Figure 9 a).

Figure 9 b) shows histograms of the number of located AE events along the x-axis direction in a cumulative manner for subsequent load cycles. The histograms are built with a 2 mm interval along the x-axis. The FPZ is defined as the zone where the histogram of the located AE events is above 15% of the maximum histogram value in the entire test, see the dotted line in Figure 9 b). An additional wherein, the width of the FPZ for each cycle is measured individually, i.e., the limit is set at

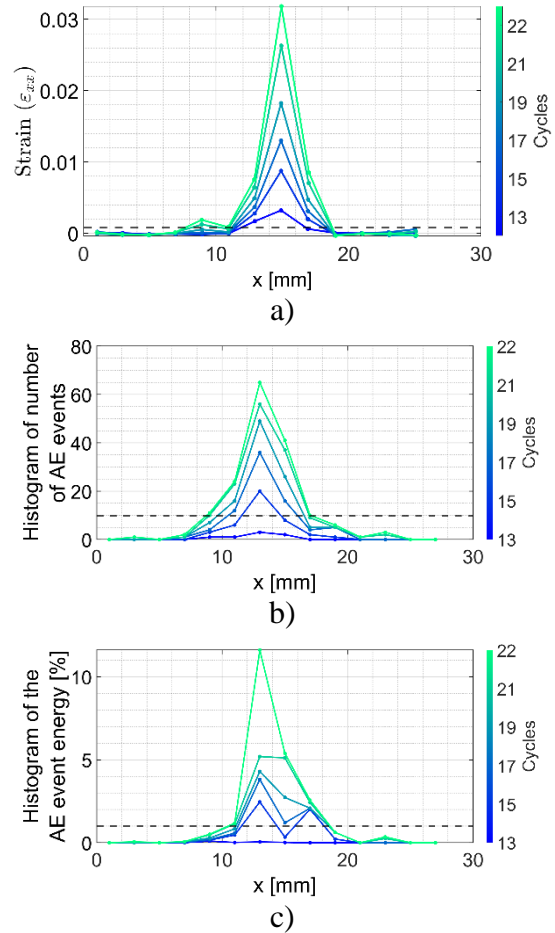15% of the maximum histogram value of each cycle.

Figure 9 Quantifying the size of the fracture process zone using horizontal strain field εxx of the DIC analysis and the AE localization plot [21].

Figure 9 c) shows the histograms of the AE energy of the located events. The FPZ is defined as the zone where the located AE events have a cumulated AE energy above 1 % of the total AE energy detected during the test. Similar to [24] only few (8 %) of the localized AE events had an energy above 1% of the total AE energy.

The evolution of the width of the FPZ (WFPZ) according to all the methods elaborated above is summarized in Figure 10. All methods show a slow increase in the width of the FPZ during the final cycles of the fatigue test. The DIC-based method results in the most stable, slow increase in WFPZ and

values are similar compared to the method in which the AE event limit is defined individually for each load cycle or the AE energy histogram is used. When defining a single limit based on the final AE event count, the result shows good agreement with the DIC-based method as the cycles progress and the number of located events increases, yet the initial values deviate largely. Generally, defining the FPZ using only the AE event count without a sufficient number of located AE events can be misleading. In such case, a better agreement can be found when incorporating AE energy information. The resulted presented are further elaborated in [21].
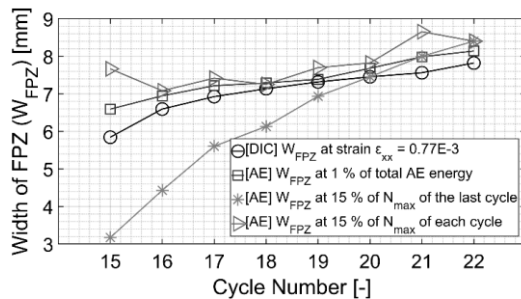

Figure 10 Summary of the width of the fracture process zone (Wfpz) computed using different DIC and AE methods. This is for the cycles in the final loading stage [21].

12 CONCLUSIONS

The evolution of damage, assessed through the cumulative number of acoustic emission events and horizontal deformation (tensile) analyzed using Digital Image Correlation (DIC), demonstrated a coherent pattern. Acoustic Emission Testing (AET) specifically detected inelastic deformations, while DIC captured both elastic and inelastic deformations. The width of the fracture process zone (FPZ) was evaluated with both AE and DIC techniques. Several methods were studied for AE-based quantification of the width of FPZ. The AE energy-based method showed a good agreement with DIC strain field based plot. The histogram plot of the AE event number also showed a good correlation with DIC results when each load cycle is treated independently and when there are sufficient number of located AE events.

REFERENCES

[1] K. Gylltoft, "Fracture mechanics models for fatigue in concrete structures," Luleå tekniska universitet, 1983.

[2] J. R. Matthews, *Acoustic Emission*. Gordon and Breach Science Publishers, 1983.

[3] N. E. Deresse, C. Van Steen, M. Sarem, S. François, and E. Verstrynge, "Acoustic Emission Analysis of Fracture and Size Effect in Cementitious Mortars," *Applied Sciences,* vol. 12, no. 7, p. 3489, 2022.

[4] C. U. Grosse, M. Ohtsu, D. G. Aggelis, and T. Shiotani, *Acoustic emission testing: Basics for research–applications in engineering*. Springer Nature, 2021.

[5] D. G. Aggelis, S. Verbruggen, E. Tsangouri, T. Tysmans, and D. Van Hemelrijck, "Characterization of mechanical performance of concrete beams with external reinforcement by acoustic emission and digital image correlation," *Construction and Building Materials,* vol. 47, pp. 1037-1045, 2013/10/01/ 2013.

[6] E. Verstrynge, K. De Wilder, A. Drougkas, E. Voet, K. Van Balen, and M. Wevers, "Crack monitoring in historical masonry with distributed strain and acoustic emission sensing techniques," *Construction and Building Materials,* vol. 162, pp. 898-907, 2018.

[7] E. M. C. a. Jones and M. A. E. Ladicola, A Good Practices Guide for Digital Image Correlation: International Digital Image Correlation Society, 2018. [Online]. Available.

[8] B. Omondi, D. G. Aggelis, H. Sol, and C. Sitters, "Improved crack monitoring in structural concrete by combined acoustic emission and digital image correlation techniques," *Structural Health Monitoring,* vol. 15, no. 3, pp. 359-378, 2016.

[9] Ł. Skarżyński and J. Tejchman, "Calculations of fracture process zones on meso-scale in notched concrete beams subjected to three-point bending," *European Journal of Mechanics - A/Solids,* vol. 29, no. 4, pp. 746-760, 2010/07/01/ 2010.

[10] Ł. Skarżyński, E. Syroka, and J. Tejchman, "Measurements and Calculations of the Width of the Fracture Process Zones on the Surface of Notched Concrete Beams," *Strain,* vol. 47, no. s1, pp. e319-e332, 2011.

[11] S. Miao, P.-Z. Pan, P. Yu, S. Zhao, and C. Shao, "Fracture analysis of Beishan granite after high-temperature treatment using digital image correlation," *Engineering Fracture*

Mechanics, vol. 225, p. 106847, 2020/02/15/ 2020.

[12] Z. Wu, H. Rong, J. Zheng, F. Xu, and W. Dong, "An experimental investigation on the FPZ properties in concrete using digital image correlation technique," *Engineering Fracture Mechanics,* vol. 78, no. 17, pp. 2978-2990, 2011.

[13] W. K. Zietlow and J. F. Labuz, "Measurement of the intrinsic process zone in rock using acoustic emission," *International Journal of Rock Mechanics and Mining Sciences,* vol. 35, no. 3, pp. 291-299, 1998/04/03/ 1998.

[14] M. Ohtsu and D. Aggelis, "Innovative AE and NDT techniques for on-site measurement of concrete and masonry structures," *RILEM State Art Rep,* vol. 20, pp. 89-103, 2016.

[15] S. Dai, X. Liu, and K. Nawnit, "Experimental Study on the Fracture Process Zone Characteristics in Concrete Utilizing DIC and AE Methods," *Applied Sciences,* vol. 9, no. 7, p. 1346, 2019.

[16] S. Y. Alam, J. Saliba, and A. Loukili, "Fracture examination in concrete through combined digital image correlation and acoustic emission techniques," *Construction and Building Materials,* vol. 69, pp. 232-242, 2014/10/30/ 2014.

[17] "CEN EN 196-1: Methods of testing cement - Part 1: Determination of strength," ed, 2005.

[18] "CEN, EN 12390-6: Testing hardened concrete - Part 6: Tensile splitting strength of test specimens ", ed, 2010.

[19] M. Thiele and S. Pirskawetz, "Analysis of Damage Evolution in Concrete under Fatigue Loading by Acoustic Emission and Ultrasonic Testing," *Materials,* vol. 15, no. 1, p. 341, 2022.

[20] H. Nasser, C. Van Steen, L. Vandewalle, and E. Verstrynge, "An experimental assessment of corrosion damage and bending capacity reduction of singly reinforced concrete beams subjected to accelerated corrosion," *Construction and Building Materials,* vol. 286, p. 122773, 2021.

[21] N. E. Deresse, M. Sarem, H. Nasser, S. François, and E. Verstrynge, "Fatigue fracture quantification in brittle cementitious materials using acoustic emission testing and digital image correlation," *Construction and Building Materials,* 2023.

[22] E. M. C. a. Jones and M. A. E. Ladicola, A Good Practices Guide for Digital Image Correlation: International Digital Image Correlation Society, 2018. [Online]. Available.